Low Cost High Speed Camera for Plasma Physics

T. Odstrčil M. Odstrčil J. Krbec L. Kocmanová
V. Svoboda
Faculty of Nuclear Sciences and Physical Engineering, CTU Prague

Abstract

A high speed low cost camera Casio EX-F1 and its possible applications have been investigated in this report. We have achieved the sampling frequency up to 40 kHz it is the effect of the way of data reading out from the CMOS image sensors called "rolling shutter". We will introduce two successful applications of this fast camera on the tokamak GOLEM. The first application is tomography and the second is visible light spectroscopy.

Keywords: high speed camera, low cost, EX-F1, tomography, spectrometer, GOLEM, rolling shutter

1 Introduction

Visible light diagnostics have been used since the beginning of magnetically confined fusion research to determine wide range of plasma parameters. The important part of many diagnostic devices is a fast linear or 2D CCD image sensor or 2D sensor. Usually, the price of this camera creates appreciable part of total device price. Moreover for many applications the speed of CCD is not height enough and if in additional to that the disadvantages of CMOS mentioned in next section do not obstruct the experiment, than this application is ideal candidate for the CMOS camera.

This report describes the high speed and low cost camera Casio Exilim EX-F1. Section 2 contains description of a basic principle of CCD and CMOS. The third section contains detailed description of EX-F1 camera. Section 4 describes the experimental setup and last section contains results and their discussion.

2 CMOS vs. CCD Chip

CCD and CMOS image sensors are used to the same purpose, both convert light intensity to electric signal, that is sampled and stored in a memory. Registered signal is proportional to the light intensity. The different are in converting of the light intensity to the electric signal.

2.1 Principle of CCD

In CCD image sensors, photons incident to silicon pixel, cause internal photoeffect and create electron-hole couple. The electrons are separated to potential well. After the exposition the charge in rows are vertically shifted per one down and last row is shifted to a readout buffer and is successively amplified and sampled by A/D convertor (Fig. 1). This way of successive shift is not suitable for high speed applications. When the total readout time is comparable with the exposure time, the light incident on CCD chip during the shift and cause image smearing. It can be solved, for example by a hidden storage area, when half of the CCD is light protected and is used as like storage [3].

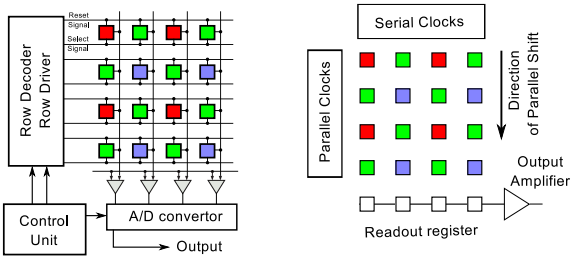

Figure 1: Schema of CMOS image sensor (left), CCD image sensor (right)

2.2 Principle of CMOS

The most important different is that the charge to voltage conversions performed in every pixel separately. The rows of CMOS array are controlled by read out and reset signal. After sending of the readout signal from control circuits, separated active pixel sensors send voltage signal proportional to registered light intensity. Voltage signal is accepted by comparators and then follow to a column-parallel A/D convertor (Fig. 1).

The advantage of this principle is definitely speed of parallel pixel read out. On the other hand, CMOS imagers are susceptible to pattern noise and common CMOS imagers have lower light sensitivity than common CCD.

2.2.1 Rolling Shutter

The most of the CMOS image sensors are equipped by column parallel readout circuits, which read simultaneously all pixels in the certain row to buffers. This way is sensor readouted, row-by-row and this non-uniform shutter is called "rolling shutter". In CMOS imagers by also integrated global shutter, but price for this is lower fill factor. Each row is controlled by a row address decoder, which sends row the reset signal and the readout signal. Because the signal is processed only by one row of readout circuits, the readout phases of different rows cannot by overlapped. If the total readout time of all rows is much shorter than the exposure time, distortion of the image, caused by sampling of different rows in different time, is negligible. However, when the total readout time is comparable or longer than the exposure time, this readout procedure cause skewness of a fast moving object in horizontal direction. On the other hand, this effect can be used to improve image quality [6]. When the last row is red out, EX-F1 camera require cca 8% of total readout time to process image. Then the readout cycle can begin again.

3 High Speed Camera EX-F1

The Casio EX-F1 is high speed digital camera for consumers product. This camera is interesting especially because of low cost. The costs is only 1000$, other cheapest high speed cameras cost more than 4000$ and cameras with comparable performance are even more expensive.

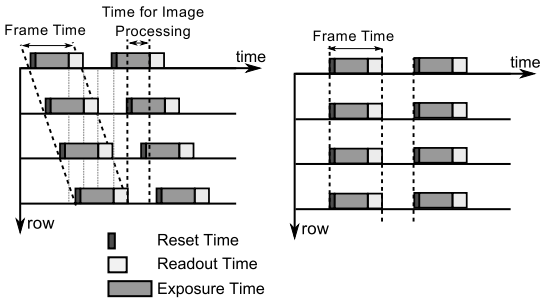

Figure 2: Timing for rolling shutter (left), global shutter (right)

Inside of the camera is 1/1.8" CMOS image sensor Sony IMX017CQE [1]. Objective is composed from 12 lens divided into 9 groups including aspherical lens. Focal length is variable from 7.3 mm to 87.6 mm, (equivalent to 36 to 432 mm in 35 mm format) and F-number is variable from 2.7(W) to 4.6(T) for widely opened aperture. Focus can be set in range 5 cm to infinity for Wide Angle and in range 90 cm to infinity in Telephoto mode. Exposure is variable in range 1/40000 s to 60 s, however only very short exposures are important for high speed applications.

There are two different ways how can be the high speed images acquired [2]. The first method is throw burst continuous shooting. This way can be achieved 60 full resolution 6 Mbit images during 1 second period. The second method is throw high-speed (HS) movies. Camera supports three different modes of HS movies - 300 fps[1], 600 fps and 1200 fps. Vertical resolution of these modes is limited by read out speed of camera, which is 125000 rows/s. Consequently, resolution of HS movies is limited to 512×384@300 fps, 432×192@600 fps, 336×96@1200 fps and hence aspect ratios are 4:3@300 fps, 2.25:1@600 fps and 3.5:1@1200 fps.

CMOS image sensor Sony IMX017CQE inside of EX-F1 is one of the fastest CMOS image sensors for standard customers. Resolution of sensor is 2916H×2178V, and thus it has resolution 6.35Mpix. Size of pixels 2.5 μm in both directions and sensor type is 1/1.8", diagonal length

[1] frames per second

9.1 mm and aspect ratio 4:3. Voltage signal can be sampled in 10 or 12 bit resolution, higher resolution is 4× slower. But HS movies and photos are stored by camera in only 8bit per color. And the last important property for high speed recording is the sensitivity. Minimal sensitivity is 4200e$^-$ at color 3200 K, flux 700 cd/m^2, exposure 1/50 and F-number 5.6 [1].

3.1 Remote Control

It is important to have remote control of camera for most of the advance applications. The camera EX-F1 can by remotely controlled in 3 different ways. The simplest way is a remote trigger, but only single or burst shooting can be triggered and camera settings cannot be set remotely. The second way is via free official remote control software [5] released by Casio. It is user friendly software with graphical interface, hence unsuitable for automated measurement controlled by scripts. And the last way is unofficial open source program [10] based on reverse engineering of Casio official control software. All of the camera parameters can be set remotely before the data acquisition and after the recording data are transferred over a USB to the computer, where are post-processed.

4 Experimental Setup

Two examples of application of this high speed camera in plasma physics will be presented in this section. Experiments were conducted on the small tokamak GOLEM located in Prague, Czech Republic [12]. The typical length of a plasma discharge is 15 ms, it is sufficiently long for usage of our HS camera.

The configurations of the cameras described before allows usage of rolling shutter effect to improve remarkably time resolution of these cameras. Read out time is 125000 rows/s, it means almost 125000 samples of plasma light per second. But shortest exposure time is 1/40000 s and therefore the observed results are averaged over at least three rows.

4.1 Tomography

The first experiment described here, is plasma tomography in visible light. It is necessary to observe plasma column from many of different lines of sight, to achieve necessary data for the tomographical reconstruction, (which is enormously badly conditioned problem).Therefore two cameras have been placed in different diagnostic ports. The first was in upper port and observed the plasma movements in horizontal direction. The second camera was situated on LFS port perpendicular to the first camera and observed the plasma movements in the vertical direction (Fig.3). Orientation of the cameras was set, so that the horizontal rows on CMOS of camera were perpendicular to the plasma column.

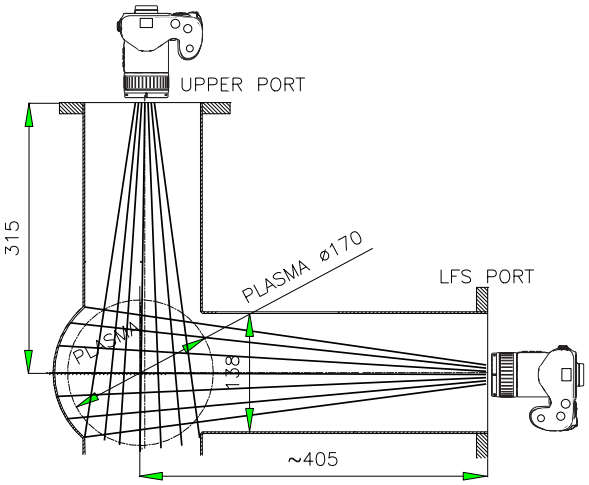

Figure 3: Poloidal cross-section of the tokamak GOLEM and the positions of the cameras during observation of plasma for tomographic reconstruction.

The main task of the plasma tomography is reconstruction of the profile of the plasma emisivity outside this chamber. Because it is ill posed and issue observed we must assume some a priory knowledge about the plasma profile. For example it is possible to add on reconstruction condition of maximal entropy or minimal Fisher information and many other [4].

Geometry of the problem is not so simple as for bolometers. Bolometers works on principle of camera obscura, so the lines of sight (called chords) from different pixels form fan with cross section in entrance slit. Thus light intensity U_i registered at certain pixel i can be calculated as path integral of emissivity $\epsilon(x, y)$ along the chords ch_i

$$I_i = \frac{1}{4\pi} \int_{ch_i} \epsilon(x(s), y(s)) \sqrt{\dot{x}^2 + \dot{y}^2} \mathrm{d}s$$

However when divergence of chords is not negligible, it is important to consider that these chords form in space pyramids with vertex in slit and hence each chord should be divided into subchords also called "virtual chords". A similar algorithm can be used for the tomographical reconstruction of the data from the camera. The only different is the shape of the chords. In this case the chords don't have pyramidal shape, but there are cones with vertex in camera focal plane. Radius of these cones depends on focal length and F-number of objective.

Up to present time, many different algorithms for plasma profile reconstruction have been developed [4, 7]. A very simple and thus popular is direct asymmetric Abel transformation [14]. But for our purpose a pixel based algorithms are more appropriate. A pixel algorithm minimalizing Fisher information [11] has been used in this paper. The speed and memory usage of this algorithm has been greatly improved [9] to allow reconstruction hundrets of chords as well as make high resolution reconstruction. High resolution is important because of minimalizing artifacts of algorithm caused by remarkable number of cords from each camera.

4.2 Spectrometer

The second example of this camera application is a simple high speed spectrometer. Figure 4 shows a schema of the light path through spectrometer. The spectrometer is composed from group of light collecting lens with 15 cm diameter and focal length 10 cm. Than the focused light beam passed throw slit and falled on a diffraction grating. We have used 1200 grooves/mm Al coated ruled grating. Reflected light was received by camera.

Similarly with the tomography, extraordinary time resolution can be obtained because of symmetry of the spectra in vertical direction. Hence it is possible to achieve maximal sampling frequency 40 kHz, however usable frequency is limited by CMOS sensor sensitivity. In comparison with other cheap (but still almost 3× more expensive) spectrometer Ocean Optics USB4000, the sampling frequency is only 1 kHz, on the other hand the rest of the properties are better. Higher time resolution

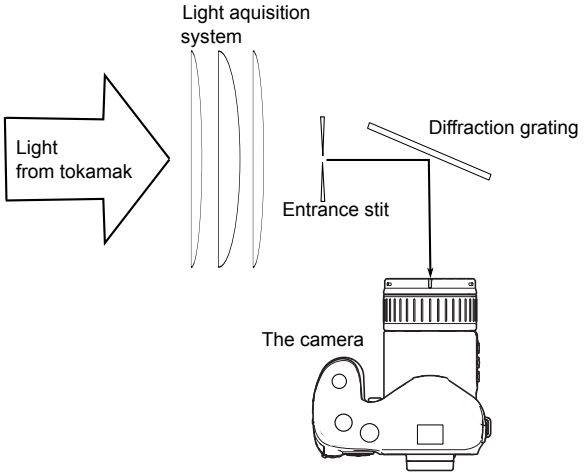

Figure 4: Schematic drawing of the low cost spectrometer

of the camera can be reached by better light collecting system that would minimalize looses during light transport and by precise aligns and focus of camera.

It is necessary to know the spectral sensitivity of camera before the measurement. In Fig. 5 is plotted sensitivity of red, green and blue colors and sum of these sensitivities. The color sensitivity depends on a white balance mode of the camera, this allow adjust of the relative sensitivity of different colors. The daylight white balance was used in all of our experiments.

The knowledge of the spectral sensitivity gives us a possibility to estimate the wavelength of an unknown spectral line. The precision of the guess can be obtained from Fig. 5. During the calculations of the Fig. 5 , the constant error 2% of maximal value 255 was expected and intensity was expected maximal possible without saturation. Near wavelength 550 nm precision almost 5 nm can be achieved.

There are another ways, how can be Fig. 5 applied. In case of only three spectral most intense lines in plasma, in different part of spectra, only the knowledge of intensities of three different colors compounds is suffice to calculate intensity of these spectral lines. Other lines must by weak enough or removed by a filter. For example H_α is the most intense red line and therefore it is possible to measure intensity of this line with both spectral and thanks to the tomography even with spatial resolution.

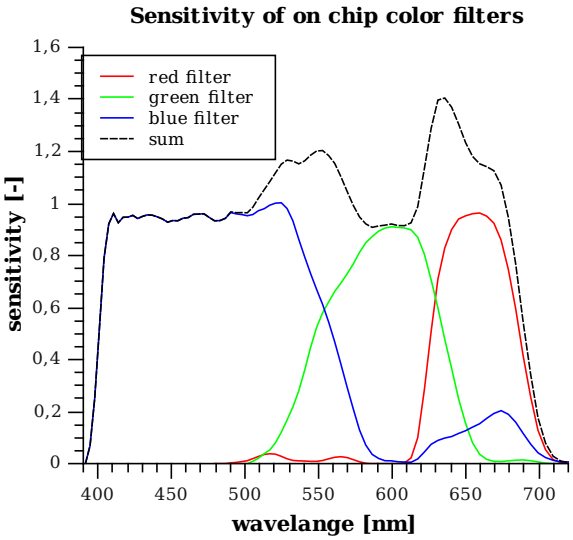

Figure 5: The spectral sensitivity of the color filters in EX-F1. White balance was set to Daylight.

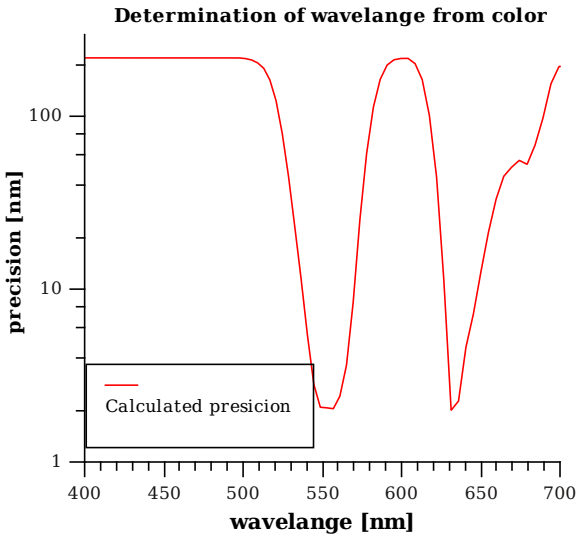

Figure 6: The estimation of the precision of wavelength, determined from Fig. 5

5 Results and Discussion

5.1 Calibration and Camera position

The focal length of the camera on LFS was set to 144 mm and focused at distance 42 cm in the center of the chamber (Fig. 3). The upper camera was set to focal length was 120 mm and objective was focused at 32 cm. The light intensity of the plasma observed from both cameras was compared and upper camera had 19% higher intensity. The aperture of the cameras were fully opened on both cameras, signal gain was set to ISO 800, exposure to 1/40000 s, white balance to daylight and HS movie mode 1200 fps. Cameras were triggered by signal from a computer, but accuracy of this triggering is worse than 10 ms. For exact synchronization with the global trigger should be used 0.5 ms long rectangular pulse from high power LED diodes, because LED diode will achieve full brightness in under a microsecond.

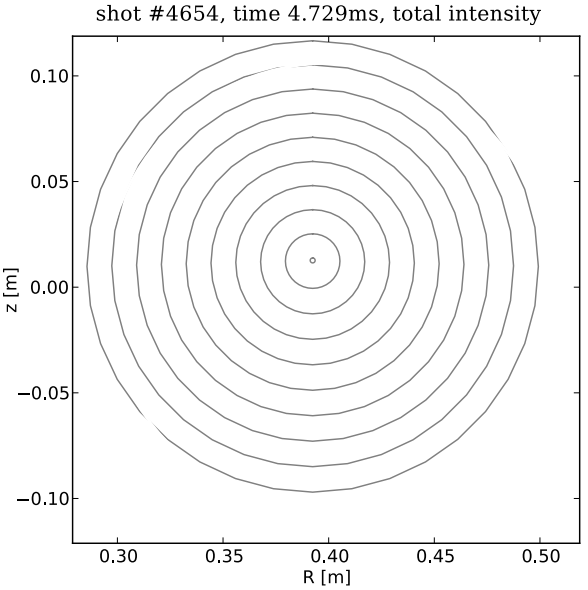

Figure 7: Profile of plasma radiation in visible spectrum reconstructed from Fig. 8, thin circles correspond to hypothetical magnetic flux surfaces and thick correspond to chamber walls.

5.2 Plasma emissivity reconstruction

Fig. 8 shows a raw data acquired from two cameras and cross-section of plasma from tomographical reconstruction of shot #4654. Unfortunately, both cameras observed only a part of the plasma cross-section, because they were placed incorrectly. It can be seen in Fig. 9, where are plotted position of

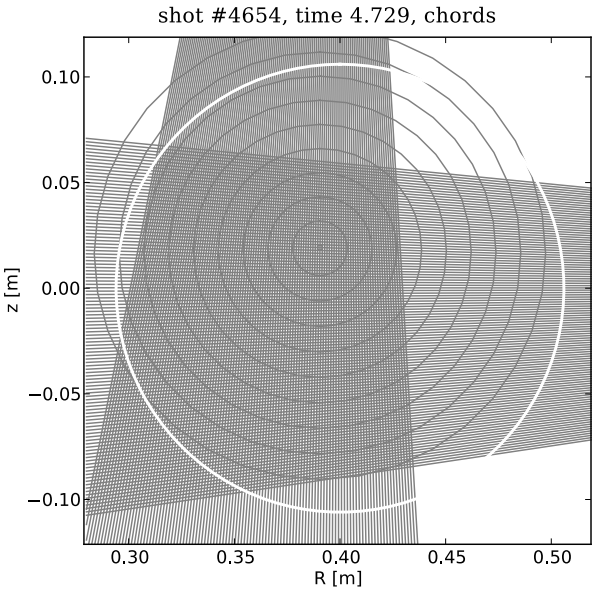

Figure 9: Positions of the chords in poloidal cross-section of the tokamak chamber

chords. The reconstructed emissivity of the latter shot at 4.7 ms is plotted in the fig. 7. The observed profile is flat or shallowly hollow but the parabolic temperature profile should cause Gaussian or sharp hollow profiles [13] of emissivity in the visible spectrum. It was probably caused by flux of neutral particles from the tokamak wall.

Neutral particles penetrate throw plasma because a mean free path of neutrals is comparable with the plasma diameter. A computer simulation of the radiation profile extraordinarily difficult, because of the unknown properties of the flux of the cold impurities. Even if the parameters of the flux were known, we would have to use a complicate radiation collision model and include anomalous transport to our calculations.

It is also possible to determine the plasma position [8] from the tomographic reconstruction or directly guess from the observed radiation. It can be used to improve and check plasma position determined from magnetic diagnostics. Great advantage of the position obtained from the radiation is that it is not integrated and there should be no absolute position shift. Disadvantage of the determination of the position from visible radiation is that the profile is flat or hollow. Better results should be obtained from bolometers that are sensitive in UV and SXR. Unfortunately, it was not possible to compare the resultes from other diagnostics, because the magnetic diagnostic was broken for all images with two cameras and bolometers are still not installed.

5.3 Visible spectrography

The low cost fast spectrometer, described in previous sections, has been used for observation of the visible plasma spectrum. Expected spectrum should contain most of the radiation (≈95%) from hydrogen, 1–5% from carbon and 0.5–1% from oxygen (from water vapors) that are common values for tokomaks. But fig. 10 shows the spectrum of shot #4614 on Golem integrated over complete shot and the result is noticeably different from the expectations. The most intensive impurities are carbon, oxygen and also nitrogen. Hence, it is obvious, that plasma was very dirty.

The time evolution of the most intensive lines are shown in Fig. 11. The time evolution had expected progress. After breakdown the H_α line rise rapidly because of plasma ionization. In 11 ms the light intensity dropped down steeply, but because the plasma current also dropped down, plasma probably hit the wall.In the third phase, the radiation from the impurities was growing up significantly to 15 ms and in the final part the light slowly decreased.

Conclusion

We have successfully confirmed potential of the high speed camera EX-F1 for application in plasma physics. These cameras have been succefully used as replacement of standard optical diagnostics on the tokamak GOLEM. The visible spectrometer and the tomography have been developed and tested on the tokamak. However the camera usage is not limited only at plasma physics, also can be used in other science branches like biology or material research and certainly in industry.

References

[1] IMX017CQE. *CX-NEWS Sony Semiconductor & LCD technologies*, 47, 2007. [online] `http://www.sony.net/Products/SC-HP/cx_news/vol47/`.

[2] EX-F1 User's Guide, 2008. `http://support.casio.com/pdf/001/EXF1_110_EU_e.pdf`.

[3] Andor. iXon EM+ Hardware Manual, 2008.

[4] M. Anton, H. Weisen, MJ Dutch, W. Linden, F. Buhlmann, R. Chavan, B. Marletaz, P. Marmillod, and P. Paris. X-ray tomography on the TCV tokamak. *Plasma physics and controlled fusion*, 38:1849, 1996.

[5] Casio. EX-F1 Controller 1.001 Software, 2010.

[6] J. Gu, Y. Hitomi, T. Mitsunaga, and S. Nayar. Coded rolling shutter photography: Flexible space-time sampling. In *Computational Photography (ICCP), 2010 IEEE International Conference on*, pages 1–8. IEEE, 2010.

[7] LC Ingesson, B. Alper, H. Chen, AW Edwards, GC Fehmers, JC Fuchs, R. Giannella, RD Gill, L. Lauro-Taroni, and M. Romanelli. Soft X ray tomography during ELMs and impurity injection in JET. *Nuclear Fusion*, 38:1675, 1998.

[8] J. Mlynář, S. Coda, A. Degeling, BP Duval, F. Hofmann, T. Goodman, JB Lister, X. Llobet, and H. Weisen. Investigation of the consistency of magnetic and soft x-ray plasma position measurements on TCV by means of a rapid tomographic inversion algorithm. *Plasma Physics and Controlled Fusion*, 45:169, 2003.

[9] M. Odstrčil and J. Mlynář. Improvements of Plasma Tomography Algorithm Based on Minimum Fisher Information. *not published*, 2011.

[10] Olsen J. S. EXF1-CTRL – Command line utility and API to control the Casio EX-F1 over USB., 2011. `http://code.google.com/p/exf1ctrl/`.

[11] C. Schlatter and J. Mlynář. Fast-Algorithm Bolometric Computer Aided Tomography (FABCAT). *CRPP EPFL Lausanne*, 2002.

[12] V. Svoboda, G. Pokol, D. I. Réfy, J. Stöckel, and G. Vondrášek. Former tokamak CASTOR becomes remotely controllable GOLEM at the Czech Technical University in Prague. In *37-th EPS Conference on Plasma Phys., Dublin*, 2010.

[13] J. Wesson and DJ Campbell. *Tokamaks*. Oxford University Press, USA, 2004.

[14] Y. Yasutomo, K. Miyata, S.I. Himeno, T. Enoto, and Y. Ozawa. A new numerical method for asymmetrical Abel inversion. *Plasma Science, IEEE Transactions on*, 9(1):18–21, 2007.

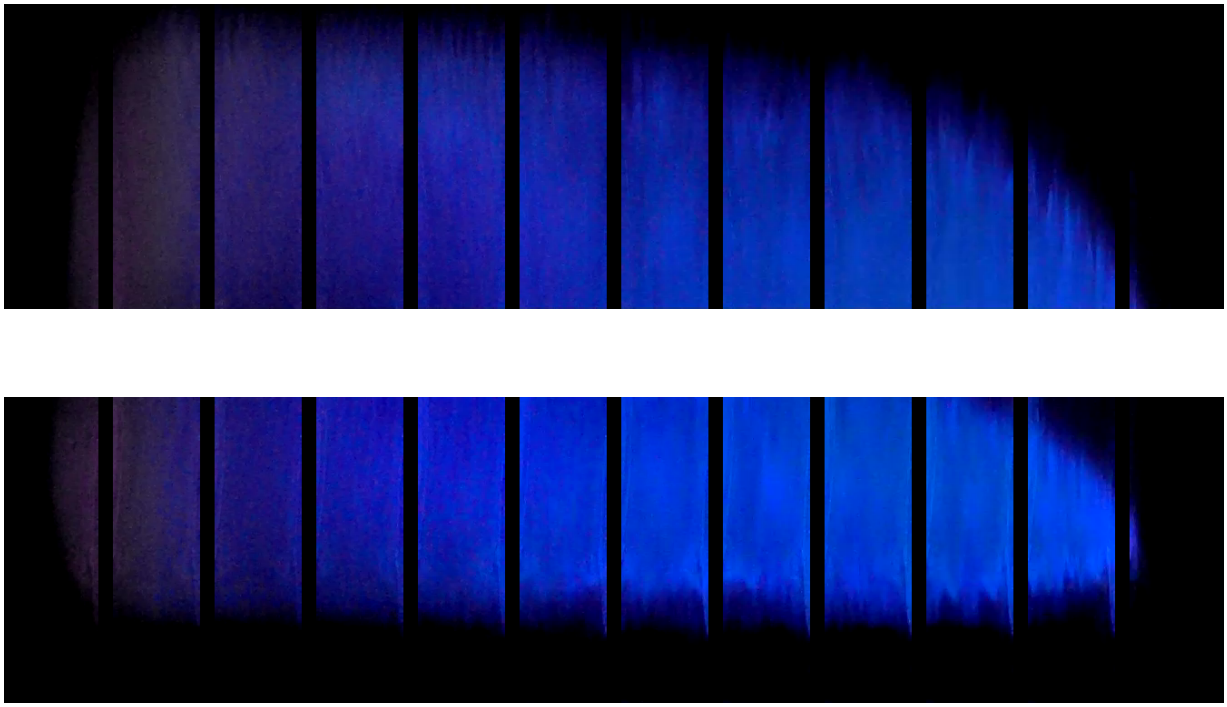

Figure 8: Raw data acquired from the cameras. The upper pictures are taken from the upper camera (Fig. 3) and the lower pictures from LFS the camera.

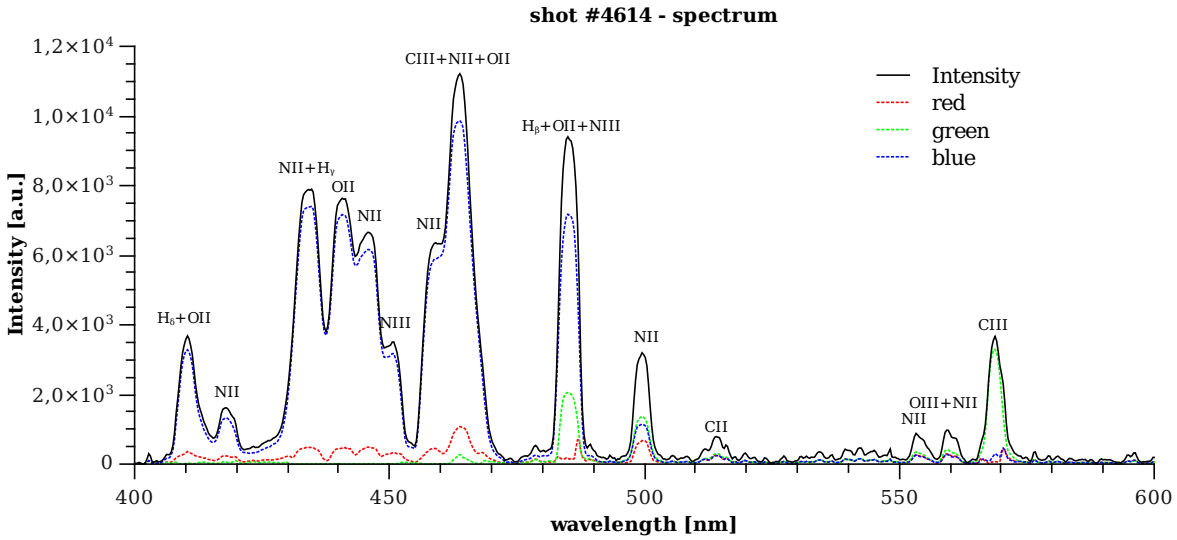

Figure 10: Visible spectrum of plasma from 400 nm to 600 nm, the signal was integrated during whole shot #4614

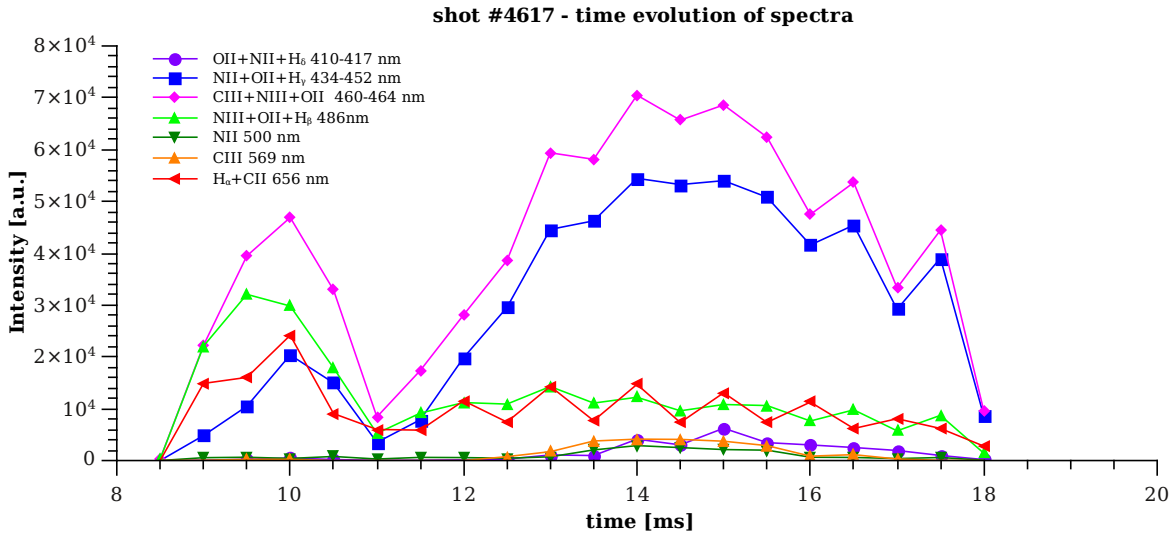

Figure 11: The time evolution of most intense lines in tokamak plasma.